Electrocompression of the Au(111) Surface Layer during Au Electrodeposition

A. H. Ayyad, J. Stettner, and O. M. Magnussen

Institut für Experimentelle und Angewandte Physik, Universität Kiel, Olshausenstrasse 40, 24098 Kiel, Germany

(Received 3 September 2004; published 18 February 2005)

In situ grazing-incidence x-ray diffraction studies of reconstructed Au(111) electrodes in aqueous electrolyte solutions are presented, which reveal a significantly increased compression of the Au surface layer during Au electrodeposition as compared to Au(111) surfaces under ultrahigh vacuum conditions or in the Au-free electrolyte. The compression increases towards more negative potentials, reaching 5.3% at the most negative potentials studied. It may be explained within a simple thermodynamic model by a release of potential-induced surface stress.

DOI: 10.1103/PhysRevLett.94.066106 PACS numbers: 68.08.–p, 61.10.–i, 68.35.Bs, 82.45.Qr

The structure of solid surfaces during chemical reactions or surface processes, such as deposition or etching, is of considerable technological interest. It has been shown that under these conditions the surface structure can considerably deviate from that found in conventional studies of the clean surface under reaction-free conditions. For example, homoepitaxial growth on Pt(111) in ultrahigh vacuum (UHV) induces the formation of a surface reconstruction, usually found only at high temperatures [1]. This was attributed to the presence of a supersaturated Pt gas phase during deposition and leads to a reentrant layer-by-layer growth in this system. Similar phenomena may occur during electrochemical processes at the solid-liquid interface, as will be shown here for the case of Au homoepitaxial electrodeposition on Au(111) electrodes in acidic electrolytes.

Au(111) surfaces under UHV conditions exhibit at room temperature the well-known herringbone reconstruction, where the topmost Au layer is 4.3% uniaxially compressed, resulting in a dislocation network structure [2,3]. The same type of reconstruction is stable at the Au(111)-electrolyte interface negative of a critical (electrolyte-dependent) potential [4–6]. The compression of the reconstructed surface layer, formed in an electrochemical environment, varies with the potential (in particular close to the critical potential), but approaches a limiting value of 4.3% at sufficiently negative potentials, i.e., is identical to that found under UHV conditions. However, an even higher compression might in principle be expected at electrochemical interfaces, since both surface stress and surface energy, which contribute to the driving force of the Au(111) reconstruction [7–10], strongly depend on the potential [8,10]. Here we will demonstrate that during Au electrodeposition indeed a significantly increased compression of the reconstructed layer can be obtained and discuss this effect by considering previous data on the potential-dependent surface stress and energy of Au(111) electrodes.

The Au surface structure was monitored *in situ* during the growth process by grazing-incidence x-ray diffraction (GID), performed at beam line ID 32 of the European Synchrotron Radiation Facility (ESRF). A Au(111) crystal (4 mm diameter, Mateck, 99.999%) with a miscut of $<0.1°$ and a mosaic spread of $0.16°$ was used, which was prepared prior to the experiments by flame annealing. The experiments were performed in solutions prepared from suprapure HCl, KCl, and H_2SO_4 (Merck), $KAuCl_4$ (Johnson Matthey), and Milli-Q water. Since the (electrolyte-dependent) stability range of the Au(111) reconstruction is ≈ 0.7 V negative of the $Au/AuCl_4^-$ equilibrium potential (0.82 V in 0.1 M HCl + 50 μM $HAuCl_4$), the deposition rate is completely determined by $AuCl_4^-$ transport in the electrolyte, i.e., by the concentration of the metal species in solution, its (temperature-dependent) diffusion coefficient in the electrolyte, and the hydrodynamic conditions. It approaches a fixed value after an initial period where a steady-state diffusion profile evolves in front of the surface. Deposition rates that are low enough to maintain a sufficiently smooth interface (see below), i.e., of ≤ 1 ML/min, can only be obtained at very low $AuCl_4^-$ concentrations (≤ 200 μM). This prohibits the use of thin-layer electrochemical cells, commonly employed in *in situ* electrochemical GID experiments [5], where transport to the surface is severely limited. Instead, a hanging meniscus cell similar to that described in Ref. [11] was used, consisting of a glass capillary filled with electrolyte and including a Pt counterelectrode and a salt bridge to a Ag/AgCl (3 M KCl) reference electrode, which establishes contact with the Au(111) electrode surface. The x-ray beam ($\lambda = 0.626$ Å) passes through the freestanding meniscus, i.e., is scattered only by the sample and the electrolyte solution. The meniscus, which is surrounded by an N_2 atmosphere to keep the electrolyte oxygen free, is stable for up to 5 h and can be maintained during the exchange of the electrolyte. As verified by cyclic voltammetry, this geometry does not inhibit $AuCl_4^-$ transport to the electrode surface and allows one to obtain high-quality electrochemical data, characteristic for a Au(111) single crystal parallel to the diffraction experiments. The hexagonal coordinate system [2,3,5] of the Au(111) substrate was used, where

$\vec{Q} = (Ha^*, Kb^*, Lc^*)$ with the lattice vectors $a^* = b^* = 4\pi/(\sqrt{3}a_0) = 2.52$ Å^{-1} parallel and $c^* = 2\pi/(\sqrt{6}a_0) = 0.89$ Å^{-1} perpendicular to the Au surface (Au nearest-neighbor distance $a_0 = 2.885$ Å). The in-plane resolution was limited by 0.5 mm slits corresponding to a detector acceptance of 0.6 mrad and by the mosaic spread of the Au single crystal.

In each GID experiment, the Au(111) surface structure was first studied in Au-free HCl, KCl, or H_2SO_4 solution, which was subsequently exchanged by a solution of the same base electrolyte containing 5–200 μM $HAuCl_4$. As a typical example, x-ray scattering data for an experiment in 0.1 M HCl with and without 50 μM $HAuCl_4$ (corresponding to a diffusion-limited Au deposition rate of $\approx$0.6 ML/min as determined from the electrochemical data) are discussed in the following. In the Au-free electrolyte, a hexagonal pattern around the integer crystal truncation rods [schematically indicated for the (0,1) rod in the inset of Fig. 1], characteristic for the electrochemically induced Au(111) surface reconstruction [4,5], is observed at potentials negative of 0.1 $V_{Ag/AgCl}$, where the reconstructed phase is stable. The relative intensities of the diffraction peaks and the in-plane reciprocal space distance δ between the (0,1) position and the reconstruction peaks (in units of a^*), which equals the incommensurability, are in complete agreement with the results by Wang *et al.* and indicative of a uniaxial incommensurate ($p \times \sqrt{3}$) structure (i.e., a "striped phase") with three symmetry-equivalent rotational domains [4,5]. According to the x-ray scattering profiles along the $\vec{q}_r$ direction $\delta = 0.0386$ at -0.3 V in 0.1 M HCl [Fig. 1(a)], corresponding to a stripe separation $p = \sqrt{3}/(2\delta)a_0 \approx 22a_0$. The intrinsic full width at half maximum of the reconstruction peak at $(H, K) = (\delta/\sqrt{3}, 1 + \delta/\sqrt{3})$ is $0.0045a^*$, from which a similar correlation length of the reconstruction domains as in Refs. [4,5] is calculated (210 ± 30 Å).

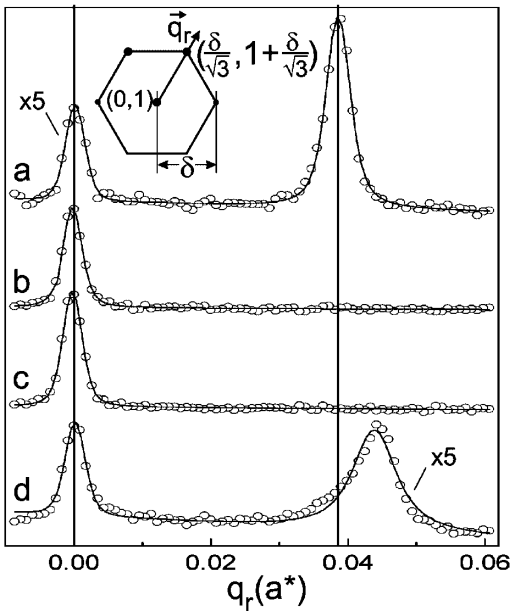

FIG. 1. X-ray scattering profiles along the $\vec{q}_r$ direction ($L = 0.15$) recorded in 0.1 M HCl at -0.3 (a) and 0.7 $V_{Ag/AgCl}$ (b) as well as after the exchange with 0.1 M HCl + 50 μM $HAuCl_4$ at 0.81 (c) and -0.3 $V_{Ag/AgCl}$ (d). Solid lines are fits of the data with two Lorentzians convoluted by a Gaussian resolution function. The inset shows a schematic diffraction pattern of the ($p \times \sqrt{3}$) reconstruction (peak intensities are indicated by the symbol size).

To study the Au surface structure during electrodeposition, the electrolyte was first exchanged with Au-containing solution under open circuit conditions within 2 to 3 min. After that, potential control was established again with the potential set to the $Au/AuCl_4^-$ equilibrium value. As indicated by the identical height of the (0,1) peak before and after the exchange [Figs. 1(b) and 1(c)], no major change in the surface roughness occurs during this procedure. Finally, Au deposition was initiated by a potential step into the stability range of the ($p \times \sqrt{3}$) reconstruction and immediately monitored by x-ray scattering profiles along $\vec{q}_r$ (with a recording frequency of 80 s per scan). In the initial profiles both the (0,1) and the reconstruction peak are very low in intensity. This is attributed to an increased surface roughness, caused by the much higher deposition rates in the first $\approx$60 s after the potential step, where the diffusion profile evolves. After 1 to 3 min, both peaks recover [Fig. 1(d)]. However, the position of the reconstruction peak (as well as of all symmetry-equivalent peaks) is considerably shifted to $\delta = 0.0445$. This shift to positive values indicates a noticeable compression of the Au surface layer as compared to Au-free solution, i.e., a smaller stripe separation p of only $\approx 20a_0$. Measurements at various q_z ($L = 0.15$ to 1.3) find approximately identical reconstruction peak intensities, indicating that only the topmost layer is compressed. A similar surface compression has until now neither been reported in the electrochemical environment nor under UHV conditions at room temperature. The reconstruction peak is considerably broadened corresponding to a decreased correlation length of 140 ± 15 Å. Its slight asymmetry may be related to increased disorder of the stripe domain phase. The integrated peak intensity in the (H, K) plane is approximately identical to that found in pure HCl solution, indicating that the surface is completely reconstructed even during deposition.

Particularly interesting is the potential dependence of the surface reconstruction during electrodeposition, which was studied by two different methods: In Au-free solutions and solutions containing 50 μM $HAuCl_4$, the potential was changed during continuous deposition in steps of typically 50 mV every 5.3 min. The peak positions were obtained from Lorentzian fits to the scattering profiles, from which the potential-dependent stripe separation p was calculated. To reduce instrumental noise and improve the fit, usually

all four profiles recorded at each potential were averaged. This method was not feasible at higher Au concentrations (i.e., higher deposition rates), where the peaks are broader, less intense, and usually vanish after ≈ 30 min deposition, probably due to surface roughening. Here each potential was probed in an independent experiment on a freshly prepared Au surface, by direct steps from the $Au/AuCl_4^-$ equilibrium potential according to the procedure illustrated in Fig. 1, and p was determined after reaching steady-state conditions . The results of such studies in HCl and KCl solutions are summarized in Fig. 2. They reveal obvious differences between the Au-free and Au-containing solutions. In Au-free electrolytes, p saturates at $\approx 22a_0$ at sufficiently negative values. Upon increasing the potential, a strong increase in p is found at the onset of the $(p \times \sqrt{3}) \rightarrow (1 \times 1)$ phase transition. Reverting the direction of the potential sweep substantial hysteresis in the stripe separation is found and $p \approx 22a_0$ is only recovered at potentials negative of -0.3 $V_{Ag/AgCl}$. This behavior is in perfect agreement with the data by Wang *et al.* [4,5]. In contrast, all experiments in Au-containing solution reveal a continuous decrease of p with decreasing potential, which is approximately linear below 0 $V_{Ag/AgCl}$ and reaches $p \approx 19a_0 = 55$ Å at the most negative potentials studied. Only close to the onset of the $(p \times \sqrt{3}) \leftrightarrow (1 \times 1)$ transition p is close to that in Au-free solution.

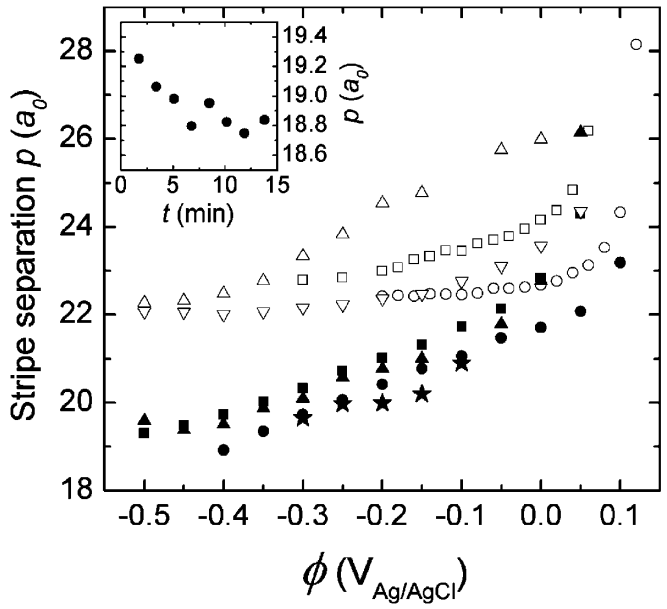

FIG. 2. Potential dependence of the stripe separation p in Au-free (open symbols) and Au-containing (filled symbols) electrolyte solution, calculated from the reconstruction peak positions. The data were obtained during stepwise potential increase (○) and subsequent decrease (□) in 0.1 M HCl, potential increase (●) and decrease (■) in 0.1 M HCl + 50 μM $HAuCl_4$, potential increase (▽) and decrease (△) in 0.1 M KCl, potential decrease (▲) in 0.1 M KCl + 50 μM $HAuCl_4$, and by potential steps from the $Au/AuCl_4^-$ equilibrium potential in 0.1 M HCl + 200 μM $HAuCl_4$ (★). The inset shows the change in p as a function of the time t after the potential step from the $Au/AuCl_4^-$ equilibrium potential to -0.4 $V_{Ag/AgCl}$.

Different electrolytes give approximately similar results, and the hysteresis between positive and negative potential sweep is comparable to that in Au-free solution. The slightly higher p values found for the potential sweeps in the negative direction may be partly caused by kinetic effects. As shown in the inset of Fig. 2, the steady-state value of p was obtained usually only several minutes after a step to more negative potentials. Averaging of the profiles may, hence, cause a small systematic error of $\Delta p \leq 0.2a_0$, which seems tolerable in view of the improved counting statistics. The p values obtained in HCl solution containing 50 μM $HAuCl_4$ (positive potential sweep) and 200 μM $HAuCl_4$, respectively, are in good agreement, taking into account the considerably higher errors for the latter ($\pm 0.4a_0$), caused by the rather low peak intensities at high deposition rates. Consequently, the potential-induced compression appears to be rather independent of the deposition rate. Furthermore, rather similar behavior is observed in HCl and KCl solutions, indicating that the compression effect is not strongly influenced by the cation species. A similar compression was also found in experiments in Au-containing 0.1 M H_2SO_4 (not shown), albeit the potential range was shifted in the positive direction due to the more positive potential of the $(p \times \sqrt{3}) \rightarrow (1 \times 1)$ transition in this electrolyte. Since the anion species is largely desorbed in the potential range of the $(p \times \sqrt{3})$ phase, this is not unexpected. Finally, the increased compression of the Au surface layer is stable against a back exchange with Au-free solution, provided potential control at a potential in the $(p \times \sqrt{3})$ regime was maintained throughout the exchange. Only after successive lifting and reformation of the reconstruction $p \approx 22a_0$ is regained.

To understand the origin of the deposition-induced compression and its potential dependence, these data are compared with previous experimental results on the Au(111) surface reconstruction and related systems. The maximum compression observed during Au deposition corresponds to a surface strain $\epsilon = -(p + 1)^{-1} = -5.0\%$, which even exceeds the value found under UHV conditions at the upper end of the temperature range, where the herringbone reconstruction is stable (865 K) [2,3]. Only the high-temperature discommensuration fluid phase exhibits higher packing densities of the Au surface layer [2,3]. The observation of a higher surface packing density during Au homoepitaxy resembles the deposition-induced formation of the Pt(111) reconstruction, found by Michely *et al.* [1]. The latter was attributed to the increased chemical potential of the Pt atom gas phase. In a similar way also, the increased surface strain in the reconstructed Au(111) surface could in principle be rationalized. However, for Au(111) homoepitaxial growth under UHV conditions,

only a $(22 \times \sqrt{3})$ phase was reported [12], which seems to rule out this explanation. Instead, we suggested that the surface compression observed during Au deposition is closer to equilibrium, whereas it is kinetically limited in the Au-free electrolyte. In the first case, the reconstruction is formed together with the growing surface layer, i.e., via attachment of atoms at the edges of growing islands. Here no (or at least a lower) barrier for attaining the energetically preferred in-plane spacing exists. In contrast, the potential-induced formation of the reconstruction in the Au-free electrolyte requires the insertion of additional Au atoms into the existing surface layer, which involves the collective motion of a large number of neighboring surface atoms and may consequently be strongly hindered.

The continuous compression of the $(p \times \sqrt{3})$ phase with the electrode potential ϕ resembles the electrocompression of underpotential-deposited (UPD) metal adlayers on noble metal electrodes [13]. However, for the Au(111) reconstruction, the change of surface strain with potential $d\varepsilon/d\phi$ is only 0.014 to 0.020 V^{-1} in the studied electrolytes at potentials sufficiently negative of the $(p \times \sqrt{3}) \leftrightarrow (1 \times 1)$ transition (i.e., in the potential range 0.0 to -0.45 V). This is more than an order of magnitude smaller than that of the UPD adlayers. As will be shown in the following, a semiquantitative description of $d\varepsilon/d\phi$ is possible within the framework of existing models of the Au(111) reconstruction. It is generally accepted that surface stress $f_{1\times1}$ as well as surface energy $\gamma_{1\times1}$ of the unreconstructed surface contribute to the driving force for the Au(111) surface reconstruction. Since both $f_{1\times1}$ and $\gamma_{1\times1}$ change with potential even in the $(p \times \sqrt{3})$ potential regime [8,10], a potential dependence of the surface strain ε is not surprising. This can be shown more quantitatively using the thermodynamic model proposed by Cammarata [7]. A combined molecular dynamics simulation and embedded-atom method (EAM) study has recently shown that this model provides a good description of the stability of fcc(111) surfaces against reconstruction [9]. In the thermodynamic model, the change in free energy per unit area associated with the reconstruction is approximately

$$\Delta F(\varepsilon) = (f_{1\times1} - \gamma_{1\times1})\varepsilon - \alpha G b \varepsilon + \tfrac{1}{2} E h \varepsilon^2/(1-\nu^2),$$

where G, E, and ν are shear modulus, Young's modulus, and Poisson's ratio, respectively, $\alpha \approx [4\pi(1-\nu)]^{-1}$, b is the magnitude of the Burgers vector, and h is the surface layer thickness (2.35 Å). The free energy is consequently minimized for

$$\varepsilon = -(f_{1\times1} - \gamma_{1\times1} - \alpha G b)(1-\nu^2)/Eh,$$

and the corresponding change of ε with potential is

$$d\varepsilon/d\phi = (d\gamma_{1\times1}/d\phi - df_{1\times1}/d\phi)(1-\nu^2)/Eh.$$

Experimental surface stress measurements in 0.1 M $HClO_4$ report an approximately linear change of $f_{1\times1}$ with potential in the $(p \times \sqrt{3})$ regime with $df_{1\times1}/d\phi \approx -0.53\ \mathrm{N\,m^{-1}\,V^{-1}}$ [8]. Using this value, the $d\gamma_{1\times1}/d\phi$ slope obtained in EAM studies ($\approx 0.045\ \mathrm{N\,m^{-1}\,V^{-1}}$) [10], $E = 81$ GPa, and $\nu = 0.41$ [7], a value of $d\varepsilon/df \approx 0.025\ \mathrm{V^{-1}}$ is found. This is only 2 times higher than our experimental data, i.e., in reasonable agreement, taking into account the simplicity of the model and the substantial uncertainties in the values for $df_{1\times1}/d\phi$ and $d\gamma_{1\times1}/d\phi$ for the systems studied here. Finally, it is noted that at the potential of zero charge [i.e., close to the potential of the $(p \times \sqrt{3}) \leftrightarrow (1 \times 1)$ transition], where the surface energy and stress should resemble most closely that of the metal-vacuum interface, the compression p during electrodeposition is almost identical to that found on clean Au(111) surface under UHV conditions. A higher compression apparently requires a negatively charged surface, which explains why this effect was not observed during homoepitaxial growth in vacuum [12]. In summary, the potential-dependent surface compression, observed in the presence of Au electrodeposition, may be viewed as a (system-independent) characteristic parameter of (negatively) charged Au electrode surfaces, which may help to refine theoretical models of the reconstructed Au(111) surface and of metal surfaces in general, respectively.

We gratefully acknowledge beam time by the ESRF, help at the ID32 beam line and technical support by J. Zegenhagen, B. Cowie, T.-L. Lee, and F. Renner, and financial support for A. H. A. from the Alexander von Humboldt Foundation.

[1] M. Bott, M. Hohage, T. Michely, and G. Comsa, Phys. Rev. Lett. **70**, 1489 (1993).
[2] K. G. Huang, D. Gibbs, D. M. Zehner, A. R. Sandy, and S. G. J. Mochrie, Phys. Rev. Lett. **65**, 3313 (1990).
[3] A. R. Sandy, S. G. J. Mochrie, D. M. Zehner, K. G. Huang, and D. Gibbs, Phys. Rev. B **43**, 4667 (1991).
[4] J. Wang, A. J. Davenport, H. S. Isaacs, and B. M. Ocko, Science **255**, 1416 (1991).
[5] J. Wang, B. M. Ocko, A. J. Davenport, and H. S. Isaacs, Phys. Rev. B **46**, 10321 (1992).
[6] D. M. Kolb, Prog. Surf. Sci. **51**, 109 (1996).
[7] R. C. Cammarata, Surf. Sci. **279**, 341 (1992).
[8] C. E. Bach, M. Giesen, H. Ibach, and T. L. Einstein, Phys. Rev. Lett. **78**, 4225 (1997).
[9] T. M. Trimble, R. C. Cammarata, and K. Sieradzki, Surf. Sci. **531**, 8 (2003).
[10] M. I. Haftel and M. Rosen, Surf. Sci. **523**, 118 (2003).
[11] Z. Nagy and H. You, Electrochim. Acta **47**, 3037 (2002).
[12] M. V. RamanaMurty, T. Curcic, A. Judy, B. H. Cooper, A. R. Woll, J. D. Brock, S. Kycia, and R. L. Headrick, Phys. Rev. B **60**, 16956 (1999).
[13] M. F. Toney, J. G. Gordon, M. G. Samant, G. L. Borges, and O. R. Melroy, J. Phys. Chem. **99**, 4733 (1995).